B. A. R C.-1010

B. A. R. C.-1010

भारत सरकार
GOVERNMENT OF INDIA
परमाणु ऊर्जा आयोग
ATOMIC ENERGY COMMISSION

MONTE CARLO CALCULATIONS OF THE RESPONSE OF AN EXTERNAL DETECTOR TO A SOURCE OF PHOTONS IN THE LUNGS OF A HETEROGENEOUS PHANTOM

by

S. Bhati, R. C. Sharma and S. Somasundaram
Health Physics Division

भाभा परमाणु अनुसंधान केन्द्र
BHABHA ATOMIC RESEARCH CENTRE
बंबई, भारत
BOMBAY, INDIA
1979

B. A. R. C. -1010

B. A. R. C. -1010

GOVERNMENT OF INDIA
ATOMIC ENERGY COMMISSION

MONTE CARLO CALCULATIONS OF THE RESPONSE OF AN EXTERNAL DETECTOR TO A SOURCE OF PHOTONS IN THE LUNGS OF A HETEROGENEOUS PHANTOM

by

S. Bhati, R. C. Sharma and S. Somasundaram
Health Physics Division

BHABHA ATOMIC RESEARCH CENTRE
BOMBAY, INDIA
1979

INIS Subject Category : C55/D15

Descriptors :

PHANTOMS

PHOTONS

POINT SOURCES

SCINTILLATION COUNTERS

LUNGS

COMPUTER CODES

RESPONSE FUNCTIONS

CALIBRATION

PLUTONIUM 238

PLUTONIUM 239

CURIUM 244

CURIUM 246

AMERICIUM 241

CALIFORNIUM 250

PALLADIUM 103

MONTE CARLO METHOD

KEV RANGE 10-100

ABSTRACT

The authors have developed a computer program to calculate the response of a 20 cm dia phoswich (3 mm thick NaI(Tl) primary detector) to a source of low-energy photons distributed in the lungs of a heterogeneous (MIRD) phantom, approximating ICRP Reference Man. Monte Carlo techniques are employed to generate photons and trace their fates in the thorax of MIRD phantom. The acceptable points of photon interactions in skeletal, lung and ordinary tissue are determined by Coleman technique. The photon interactions considered are photoelectric and Compton. The calculations yield the exit photon energy spectrum which is smeared with experimentally determined Gaussian resolution function to convert into pulse-height spectrum observable with the detector. The computer program has provisions for incorporating the effects of iodine K x-ray escape as well as variable intrinsic efficiency of the detector.

Computed calibration factors (cpm/μCi integrated over the full spectrum) are given for the phoswich located centrally over and in contact with the chest for several low-energy photon sources distributed uniformly or as points in the lungs of the phantom. The radionuclides considered are ^{238}Pu, ^{239}Pu, ^{241}Am, ^{244}Cm, ^{246}Cm, ^{250}Cf and ^{103}Pd. Examples of generated exit photon and the corresponding pulse-height spectra are included. The spectral changes observed in these generated spectra, which are also discerned in experimental pulse-height spectra, are discussed in detail. Thus, we observed photopeak energies of 18.4 and 55.5 keV for U_L X-rays and ^{241}Am gamma-rays respectively. It is shown that consideration of the total (i.e. both uncollided and those escaping after collision instead of the uncollided alone) flux of escaping photons improves the calibration factors by about 50 % for ^{239}Pu, 70 % for ^{103}Pd and as much as 340 % for ^{241}Am gamma-rays. In addition, calibration factors are calculated for point ^{239}Pu sources located at different sites in the phantom lungs and data on the escape efficiencies are presented. The suitability of the MIRD phantom as a calibration device for low-energy photon in-vivo spectrometry is examined in the light of these results.

MONTE CARLO CALCULATIONS OF THE RESPONSE OF AN EXTERNAL DETECTOR TO A SOURCE OF PHOTONS IN THE LUNGS OF A HETEROGENEOUS PHANTOM

by

S. Bhati, R.C. Sharma and S. Somasundaram

INTRODUCTION

Many laboratories have set up facilities for the assessment of low-energy photon emitters in-vivo using external detectors (Go76; Sh76; To76). Dual scintillators (phoswich) in various sizes have emerged as the detector of choice for the assessment of chest burdens of certain actinides (Ne78a). Such measurements rely on the detection of L x-rays or low-energy gamma-rays near the surface of the chest. The transmission of low-energy photons through chest would depend on the total thickness of tissue in their path. The emerging photon spectrum of gamma-rays of initial energy greater than 30 KeV would also exhibit the prominent observable features of Compton scattering. The calibration factor (expressed in counts/photon or cpm/μCi of activity) for the phoswich detector used for assessing lung burden of an actinide is likely to have certain inherent uncertainties, depending upon the distribution of the radioactive aerosol in the lungs. Although it may appear that an in-vivo calibration procedure involving inhalation of a suitable simulant of the actinide by human volunteers would not necessitate a knowledge of the actual distribution of the radionuclide, it would not be wholly correct to assume that the calibration factor so obtained would be valid for all times since the radionuclide may with the passage of time redistribute itself within the lungs in an unknown manner (Vo76). Moreover, the in-vivo calibration techniques for ^{239}Pu, adopted in our laboratory and elsewhere, requiring the inhalation of mock-Pu (not always an exact simulant of the actinide) aerosol by human volunteers need an additional exercise of deriving the calibration factor for ^{239}Pu from that of the simulant (Ne78b). Experimental information on the calibration factor and the extent of its variability could only be obtained resorting to the difficult and tedious task of designing a realistic chest phantom and simulating various kinds of source distributions within the lungs (De76). Alternatively, theoretical methods of calibration may provide this information for a range of actinides and may supplement the limited amount of experimental data. The semi-empirical calculational methods (e.g. Ju72) which are applied to calibrate whole-body radioactivity counters for high-energy photon emitters use homogeneous phantoms and their extension to the low-energy domain (< 100 KeV) would be grossly invalid. A heterogeneous phantom whose organs are characterised by mathematical expressions would be an ideal propo-

sition. Monte Carlo techniques may be employed to solve photon transport problems in the selected mathematical phantom. The correctness of the results would depend upon the realistic nature of the phantom.

Working on these lines, our effort has resulted in the development of a computer program which predicts the pulse-height response of an external detector to a source of low-energy photons (10 KeV < E < 100 KeV) distributed in a selected manner in the lungs of a heterogeneous mathematical phantom. The corresponding photon spectrum of the emergent radiation and the calibration factor for the selected detector-phantom geometry are obtained. The mathematical phantom, the schematics of the computer program and the results of calculation are discussed in the report. We examine also the suitability of the selected phantom for calibration in low-energy photon in-vivo spectrometry.

MATHEMATICAL PHANTOM

Two kinds of mathematical simulations of chest phantom suitable for use exist. Falk (Fa74) has developed a model which describes the lungs and chest of an exposed subject by a set of parameters which can be altered to simulate varying body stature and chest thickness. He used this model to obtain the calibration factors for low-energy photon emitters in lungs containing a point source. This method has certain limitations. Firstly, it is designed for measurement of the uncollided photons without any consideration of the Compton scattering effect which dominates in tissue-equivalent media at photon energies greater than 30 KeV. Secondly, the calibration is obtained for point source locations only which are considered as equivalent to uniform spherical distributions.

Another, more promising, mathematical phantom has been described by Snyder et al (Sn65). The phantom described by them is supposed to approximate ICRP Reference Man closely and has been used by them to calculate photon absorbed fractions. It has a simple geometrical shape and takes into account all the major organs of the body which are characterised by suitable quadratic equations. Though each organ in the phantom is homogeneous in composition and density, the phantom itself is heterogeneous in nature since different compositions and densities are assumed for the skeletal region, lung tissue and the rest of the phantom. The geometrical outline of the phantom, together

with an elaboration of the constitution of the chest region, is shown in Fig. 1. Due to the specificity, definiteness and successful use of this (MIRD) phantom in providing theoretical estimates of photon absorbed fractions, we have investigated it in our study to derive calibration factors for low-energy photon emitters in-vivo. Since our interest centers on the chest region only, we have used the relevant organs in this region, viz. lungs, ribs, heart (taken to be ordinary tissue) and spine. The corresponding equations have been taken from Snyder et al (Sn65).

MONTE CARLO COMPUTATION SCHEME

The Monte Carlo transport technique consists in tracing the fates of a large number of photons in the given media. Beginning from the source, namely, lungs, each photon is followed up individually within the chest region of the phantom, simulating its interactions with the materials of the heterogeneous phantom. Since the quantity of interest here is the energy distribution of photons falling on the face of the detector kept at a specified position on the chest of the phantom, it simplifies the Monte Carlo treatment to some extent, in the sense that a calculation of energy deposition within the phantom materials is not needed, as in absorbed fraction calculations. In Fig. 2 we present the flow chart schematic of the computer program employed to compute the exit photon spectrum and the corresponding observed pulse-height response of the phoswich detector from the thorax of the MIRD phantom for a photon emitter present in the lungs.

The program designed for BESM-6 computer at Trombay begins by choosing an appropriate Cartesian coordinate system (X,Y,Z)all in cm) shown in Fig. 1. The origin is located at the centre of the base of the torso, with positive Z-axis, positive Y-axis and positive X-axis directed towards head, posterior and left side of the phantom respectively. The generation of source photons of selected energy in lungs is carried out according to the source distribution desired to be simulated. Two kinds of source simulations are available: (a) An isotropic point source at a given point in the lung is simulated by choosing the direction cosines (U,V,W) in a random fashion; (b) Uniformly distributed source in the lung is simulated by generating photon sites at random within the bound volume of the lung — both position and angular coordinates are selected in a random fashion. In case a source with photons

of more than one energy is to be simulated, the energy parameter of the source photons is selected randomly in accordance with the known yield values of photons of different energies. Having generated a well-defined photon for the selected source distribution, it is followed in the heterogeneous media consisting of lung tissue, skeleton and the rest of ordinary tissue, to determine its point of interaction.

Here onwards we need to know the attenuation coefficients (μ) of the three media at the photon energies of interest. These constitute an important parameter for the Monte Carlo calculations. The total (μ_t) and photoelectric (μ_p) mass attenuation coefficients for water (assumed as tissue-equivalent) and bone used in the present work are given in Table 1 (Hu69). The cross-section for the Compton process is taken as the difference between these two cross-sections at the given photon energy. Table 1 indicates also how the relevant photon cross-section data for lung tissue are obtained. We found that the cross-section data for photoelectric process given in Table 1 produced almost a straightline when plotted against photon energy on a log-log graph. Linear interpolation of μ with E would yield slightly higher values of cross-section data at intermediate photon energies, especially at energies below 30 KeV, than those obtained by the use of ln μ vs ln E plots (Table 2). We therefore employed the latter form of plot whenever cross-section data at any photon energy intermediate to those given in Table 1 were desired.

At the energy of the photon under consideration the total attenuation coefficients of the three different media assumed to be present in the phantom differ widely. A suitable method is required to determine an acceptable point of interaction. A technique given by Coleman (Co68) is used for this purpose. In this technique we first find three values of the total linear attenuation coefficients corresponding to the three media at the energy of the photon being followed. We then select the maximum (T_{max}) of the three attenuation coefficients. The path length S from the starting point of the photon to a probable point of interaction is next calculated by sampling the exponential distribution of photon intensity, i.e. $S = - \ln(R1)/T_{max}$, where R1 is a random number between 0 and 1. A check is then made to see whether this probable interaction point is inside or outside the trunk region of the phantom. In

the latter case the unattenuated and uncollided photon finds its way out of the phantom. In the former case, since the coordinates of the interaction point are known from the calculated pathlength (S), the phantom medium which contains it is found out. Denoting the total linear attenuation coefficient of this medium by TX, the ratio RTO = TX/Tmax which indicates the probability of the interaction point being real and acceptable, is ascertained. Thus, if RTO = 1, the interaction point is considered a valid one but if RTO < 1, its validity has to be ascertained. For this verification we generate a random number R2 between 0 and 1 and accept the interaction point as real and valid only if R2 < RTO. Otherwise, the interaction point is considered unreal and the photon is given another flight from the point already reached in the same direction with the same energy and a fresh point of interaction is found.

The type of interaction is then determined by random sampling from the possible interaction processes, namely, photoelectric and Compton in proportion to their individual probabilities. The relevant photon cross-section data from Table 1 were used. Since any photoelectric event amounts to complete absorption of the photon in the medium at the point of interaction, it would not contribute to the exit photon spectrum. Such a photon is terminated and a fresh history is started. In the case of a Compton scatter event, the energy of the scattered photon is calculated by sampling the differential Klein-Nishina cross-section for free electrons using a method described by Cashwell and Everett (Ca59), i.e.

$$E' = \frac{E}{1 + Sr + (2E - S)r^3}; \qquad S = \frac{E}{1 + 0.5625E}$$

E and E' are the energies in terms of electron rest mass ($m_o c^2$) of the initial and the Compton scattered photons respectively and r is a random number between 0 and 1.

The polar angle (θ) of the scattered photon between 0 and π is then calculated from the relation

$$\cos\theta = 1 + 1/E - 1/E'$$

The azimuthal angle of the scattered photon is determined from random sampling in the interval from 0 to 2π. From these the new direction cosines of the scattered photon with respect to the original coordinate system are computed (Ca59) and the scattered photon is again followed as any fresh photon

until it is either absorbed photoelectrically or its energy falls below 10 KeV when it is terminated and a new photon history is started. At the outset or at any stage of the history, if the photon is found to exit from the thorax phantom (interaction point is outside), it is categorised and stored in a suitable energy bin of the exit photon spectrum according to its energy only if it falls on the detector face.

Since at low photon energies photoelectric interactions would be more dominant and probable, only a small number of such photons would make their way to the exit photon spectrum, although the initial number of photons may be very large. This would mean poor statistics. In the present program the only provision to improve this situation is the usage of a very large number (60,000) of initially generated photons.

The result of these Monte Carlo calculations is the energy spectrum of photons emerging from the thorax phantom, a part of which falls on the detector. In practice, however, two detector variables lead to a modification of the original exit photon spectrum. One of them is the variation of the intrinsic efficiency of the detector with photon energy and the other is the effect of iodine K x-ray escape probability for photon energies exceeding 33 KeV. These variables are known as a function of photon energies for 3 mm thick NaI(Tl) detector (Sh72a).

The effect of variable intrinsic efficiency has been incorporated by multiplying any peak area with the actual intrinsic efficiency value at the mean peak energy. The simulation of the effect of the iodine escape has been included in the computer program as follows: From the counts of each channel in the exit photon spectrum (E > 33 KeV) from the thorax phantom, a quantity equal to the multiplication of each channel counts with the corresponding escape probability is subtracted and the same is added to a channel at energy (E - 28) KeV. The values of escape probability at several energies for good geometry, given in Table 3, are taken from Sharma et al (Sh72a) and linear interpolation is used to get values at intermediate energies. Thus a modified exit photon spectrum results which takes into consideration both the variables mentioned above.

The role of the detector essentially is to smear the exit photon spectrum into a pulse-height spectrum. This is achieved in practice by

smearing the photon spectrum with the experimentally determined Gaussian resolution function characterising the detection system. Experimental measurements with the 20 cm dia phoswich detector at four photon energies below 100 KeV indicated that the standard deviation (σ) of the Gaussian peak can be expressed as

$$\sigma(E) = A\sqrt{E} + B$$

The constants A and B were determined from a fit of the experimental data, $\sigma(E)$ vs $\sqrt{E}$.

Having known $\sigma(E)$ as a function of photon energy, the contribution B(K,J) from the Kth channel of the exit photon spectrum to the Jth channel of the smeared pulse-height spectra is given by

$$B(K,J) = \frac{A(K)}{\sigma_K\sqrt{2\pi}} \int_{C(J-1)}^{C(J)} \exp\left[-\frac{(E-E_K)^2}{2\sigma_K^2}\right] dE$$

where A(K) is the number of photons in the Kth channel of the exit photon spectrum having E_k as the corresponding mean energy. C(J) and C(J-1) are the upper and lower energy limits of the Jth channel of the smeared pulse-height spectrum and σ_k is the standard deviation of the Gaussian peak at energy E_k in the pulse-height spectrum. Using normal probability function P(X)

$$B(K,J) = A(K)\,[P(X_2) - P(X_1)]$$

where $X_1 = \dfrac{C(J-1) - E_k}{\sigma_k}$ and $X_2 = \dfrac{C(J) - E_k}{\sigma_k}$.

$\sum_{k=1}^{n'} B(K,J)$ would be the contribution from the whole of the exit photon spectrum to the Jth channel of the pulse-height distribution. Counts in the channels J = 1, ... n give the complete pulse-height spectrum. The procedure of "linearisation of peak channel counts" (Zi61) has been incorporated to locate the peak position in the pulse-height spectrum.

RESULTS

The computer program described above was used to get the following results:

A. Generate exit photon spectra and the corresponding observable pulse-height response for a phoswich detector for several actinides, viz. ^{239}Pu,

^{238}Pu, ^{241}Am, ^{244}Cm, ^{246}Cm, ^{250}Cf and the electron capture radionuclide ^{103}Pd, present in the lungs of the MIRD phantom. Table 3 lists the data on x-ray energies and their abundances in percentage of disintegrations of the parent nuclide assumed in these calculations. Two kinds of source distributions of these radionuclides in the lungs are considered — point and uniform. Five points on the semi-Z axis of the half-ellipsoid representing the left lung were defined as upper one-fourth (S1), centre (S2), lower one-fourth of semi-Z axis (S3) and at top (ST) and bottom (SB) of lung at Z-axis. In one instance a point source was assumed to be present at locations S1, S2 and S3 in succession while the detector was positioned on the thorax with its centre right above the three locations. In another instance a point source at all the five locations and a single 20 cm dia phoswich (3 mm NaI(Tl) primary detector) located centrally over the upper region of the thorax with the detector edge 0.3 cm below the bottom of the first rib was assumed. Together with uniform source distribution these situations would provide useful data on the extent of variability of the calibration factor as a function of source distribution in a normal MIRD phantom. Data are also given for a two detector geometry shown in Fig. 1. Several examples of the predicted pulse-height spectra are included and the calibration factors are tabulated and comparison is made with the limited amount of experimental data available.

B. The effect of the presence of rib bones on the transmission of low-energy photons (U_L x-rays) was also seen. In addition, data similar to those in (A) were generated for different densities of lung tissue varying in the range 0.1 - 0.4 g/cm^3.

C. Calibration factors (counts/photon) were obtained for the detector for the counting geometry described in (A) at several photon energies from 20 to 170 KeV for uniform source distribution in the lungs of the MIRD phantom. These results are also presented and comments are made about the effects of forward and backward scattering by tissue-like media on the spectral shapes of these photon sources on the basis of the generated data,

D. We present also the generated data on escape efficiencies of 16, 53, 70 and 185 KeV photons from different parts of the MIRD phantom for uniform source distribution in the lungs.

DISCUSSION

Shapes of Generated Spectra

Fig. 3(a-e) depict the exit photon spectra as histograms and the resultant pulse-height responses of the phoswich detector as smooth curves for the actinides, ^{239}Pu, ^{238}Pu, ^{241}Am, ^{244}Cm, ^{246}Cm, ^{250}Cf and the electron capture radionuclide ^{103}Pd, distributed uniformly in the lungs of MIRD phantom and a single phoswich (20 cm dia) detector positioned centrally over the thorax, as described earlier. For all the results presented in these figures the photon energies and intensities given in Table 4 were used, starting with 60,000 initial photon histories of each energy and the results were combined in proportion to the respective photon yields for each radionuclide. In the case of U_L x-rays, the contribution to the exit photon spectrum from 13.6 KeV energy was verified to be negligible (Sh72b; Sh74); hence the pulse-height spectrum shown in Fig. 3a comes entirely from two components, viz. 17.2 and 20.2 KeV photons emerging uncollided or after collision. More noteworthy here is the buildup factor defined as the ratio of the total number of photons to the uncollided ones in the exit photon spectrum (Fig. 3a, b, d) obtained from the MIRD phantom since it shows the contribution from scattering within the phantom at such low energies. It is found that the buildup factor for U_L x-rays from ^{238}Pu and ^{239}Pu is about 1.5 which increases to 1.7 for Rh_K x-rays. The buildup factor is dependent on photon energy, the position of the detector over the thorax and the selected energy threshold of the detection system. These results show that Compton scattering effects cannot be neglected in any type of calculations, whether using Monte Carlo techniques or any semi-empirical approach aimed at obtaining the calibration factors. If the uncollided flux of photons alone is considered, an under-estimation in the calibration factor would result for the selected detector-phantom geometry and source distribution in the lungs of the phantom. For photons of initial energy < 30 KeV, Compton scatter does not reduce the photon energy appreciably and even if the channel width in the exit photon spectrum is 0.6 KeV/channel, the maximum channel contents will include some scattered photons. It would be incorrect to assume the maximum channel contents as equivalent to the number of uncollided photons. Thus, correct estimates of the buildup factors cannot be worked out straightaway from the data shown in Fig. 3(a-e).

It is apparent from Fig. 3a that the pulse-height spectra corresponding to the exit photon spectra of U_L x-rays emerging out of the phantom indicates a photopeak energy at 18.4 KeV whereas the average peak energy expected from a bare source is about 17 KeV. This shift in photopeak energy to the higher side is due to the different proportions of transmitted photons of two energies and is a consequence of the rapid variation of the linear attenuation coefficients of tissue at low photon energies. Similar observations have been made in experiments (Sh72b; Sh74). Fig. 3(c, d, e) illustrate similar spectral effects in the case of ^{244}Cm, ^{246}Cm, ^{103}Pd and ^{250}Cf, the shifted photopeak energies being 19.5, 19.5, 20.6 and 20.3 KeV respectively. Thus the computer program appears to regenerate the spectral shapes of these low energy (E < 33 KeV) photon emitters present in the lungs of the phantom. These peak shifts offer a method of estimating the effective depth of the source in the phantom in the region viewed by the detector.

Fig. 4 shows a result similar to those presented in the previous figures but for a source of monoenergetic photons of energy 40 KeV (i.e. E > 33 KeV) distributed uniformly in the lungs. Two points are worth noting in this figure. The effect of the iodine K x-ray escape is the appearance of a photopeak at 10.4 KeV and the figure illustrates how the computer program is able to take care of this effect. The photopeak has shifted downwards to 37.7 KeV from the initial energy of 40 KeV. Although the exit photon spectrum shows an overwhelmingly large number of events at 40 KeV, the subsequent interaction of the exit photon spectrum with the detector, assuming 100 % intrinsic efficiency, leads to a peak at a lower energy.

We had earlier applied Monte Carlo techniques to predict the magnitudes of changes in pulse-height spectra of monoenergetic low-energy photon (E < 100 KeV) emitters embedded under tissue-like media (Sh76b; Sh77). Downward shift of photopeak energy and deterioration of energy resolution of the detection system were the spectral changes considered. Predictions were made for a thin (10 cm dia x 5 mm thick) NaI(Tl) detector and for point photon sources located on the axis with the absorber-scatterer medium interposed between the source and the detector. Forward scattering of quanta alone was then taken into consideration. These studies showed that in addition to the electron density of the absorber-scatterer medium, the finite energy resolution of the detector

is a dominant factor in inducing spectral changes and that an ideal detector with an infinitely fine resolution would not exhibit such effects.

We have now performed similar calculations for the 20 cm dia phoswich detector with water and perspex as absorber-scatterers. In addition, we have investigated the effect of backward scattering on spectrum shapes. Fig. 5 a & b summarise the results of calculations for 60 KeV photons and show the variation of energy band ratio as a function of absorber-scatterer thickness, a constant thickness being present at the back of the source. The energy band ratio is defined as the ratio of counts in (45-60 KeV) energy band to counts in (60-75 KeV) energy band, calculated from the predicted pulse-height spectra. The energy band ratios are different for water and perspex. For a fixed thickness in front, a higher value of the energy band ratio is predicted, depending on the thickness at the back. This effect of back-scattering appears to saturate for water thicknesses in excess of 5 cm at the back of the source. The variation in energy band ratio is a direct consequence of the downward shift of photopeak since a linear relation exists between the two. This emphasis on the energy band ratio is due to its ease of calculation. An obvious implication of these results would be the determination of the effective depth of an ^{241}Am source in vivo. A maximum error up to 4 cm in depth determination would occur if no account is taken of the back-scattering effect. Another point which emerges is that the so-called tissue-equivalent materials (water, perspex etc.) differ from each other insofar as their effect on the spectrum shapes of low-energy photon emitters are concerned (Sh76b). This brief discussion would be helpful later on when we derive the effective depth of source in the MIRD phantom from the generated spectra for 60 KeV photons.

Calculated Calibration Factors

In Table 5 we present the calculated calibration factors for a single 20 cm dia phoswich detector placed centrally over the chest of the MIRD phantom for two kinds of source distribution in the lungs. It will be observed that the calibration factors for uniform distribution are slightly higher for ^{239}Pu, ^{238}Pu, ^{244}Cm, ^{246}Cm, and ^{250}Cf, similar for ^{103}Pd and lower for ^{241}Am gamma-rays than those obtained for a point source located at the centre (±8.5, 0, 55.5) of each lung. This might suggest that the effective depth of the point

source is slightly greater than that in the case of uniform distribution. However, the effect of severer attenuation initially is more than compensated by Compton scatter in the case of photons of energy greater than 20 KeV. It may therefore be not advisable to replace a uniformly distributed source by a point source at the centre of the lung for all photon energies.

Table 6 lists the calculated calibration factors for ^{239}Pu and ^{103}Pd point sources at three well-defined points in the left lung and a single detector of stated diameter placed right over the point source such that the line joining the detector centre and the point source is parallel to Y-axis. Table 7 lists the calculated calibration factors for a point source located at ST, S1, S2, S3 and SB (coordinates are given in the table) and a 20 cm dia phoswich placed centrally over the chest. For the above source locations the calibration factors are in the ratio 1:218:407:368:58 and 1:8:20:15:4 for ^{239}Pu and ^{103}Pd respectively. These data bring out the extent of variability in the calibration factors. The data presented in Tables 6 and 7 clearly suggest that low-energy photons are more severely attenuated in the upper half of thorax than in the lower half. Available experimental data on humans do not support this.

Fig. 6 shows the variation of the calibration factor (count/photon) of a 20 cm dia phoswich placed centrally over the chest of the MIRD phantom containing a uniform distribution of photon sources in the lungs. The utility of this graph lies in prediction of calibration factors for several radionuclides. This is done by either reading or calculating from the given polynomial expression the calibration factors for the desired photon energies and then summing them up in proportion of the photon intensities, obtained from the decay scheme of the radionuclide.

We studied also the effects of different lung densities and of replacement of rib bones by ordinary tissue. For the case of uniform source distribution, lung densities of 0.1 and 0.4 g/cm^3 gave calibration factors for ^{239}Pu 80 % higher and almost similar respectively to that given in Table 5, while replacement of rib bones by ordinary tissue almost doubled it.

Photon Escape Efficiencies

For a selected low-energy photon emitter distributed in the lungs of the phantom, it might be of interest to know the photon escape patterns

from front, back and the sides of the phantom. The escape efficiency is defined as the percentage of the photons that escape either uncollided or after collision. To determine the escape efficiency, the phantom thorax was enclosed in a parallelopiped of minimum size and the photons escaping from the thorax and hitting the different surfaces of the parallelopiped were recorded. Our procedure was similar to that adopted by Scott et al (Sc77) who have presented escape efficiencies for uncollided photons only. With the computer program described earlier in this paper we determined escape efficiencies for the total flux of escaping photons, i.e. both uncollided and those escaping after collision. The results of our calculation together with the results of Scott et al for the case of uniform distribution of source emitting photons of initial energies 16, 53, 90 and 185 KeV are presented in Table 8. These photon energies are selected for the sake of comparison.

In the case of 53, 90 and 185 KeV photons, the uncollided fraction is about one-third of the total flux of escaping photons. If one takes account of the uncollided photons only, an under-estimation by similar magnitude in the calibration factor might be expected. It appears that the total flux of 16 KeV photons escaping from the back may be slightly higher than from the front. Our values of the escape efficiency for uncollided photons are slightly lower than those reported by Scott et al due perhaps to use of different cross-section data. The inclusion of photons escaping after collision does not seem to alter the qualitative picture of escape efficiencies and there appears to be good agreement in the patterns of escape efficiencies calculated by us and those presented by Scott et al. This similarity strongly suggests the confirmation of the conclusions of Scott et al (Sc77) regarding the optimum detector size and placement for low-energy photon in-vivo spectrometry, although available experimental data on humans do not support them.

Body Build Parameters

The calculated calibration factors would be valid only for body builds typical of the MIRD phantom. Hence the body build of the MIRD phantom needs to be defined. The relevant parameters normally chosen for such purposes are chest wall thickness (CWT) or effective soft tissue thickness (ESTT). CWT is generally measured by ultrasonic methods (Ga77; Ha77), being the average (exponential or arithmetic) of tissue thicknesses between the lung surface

are points on the chest surface in the intercostal spaces between the ribs, lying within the area viewed by the detector. From the quadratic equations describing the lungs and the thorax we calculated the thicknesses at 19 points within the mentioned region of the chest of MIRD phantom. The arithmetic and exponential averages of these thicknesses were found to be 3.64 and 3.2 cm respectively. If CWT for the phantom is calculated from published correlations (Ha77) with weight/height ratio, a value of 2.32 cm is obtained. Since the MIRD phantom is supposed to represent a 70 Kg man, the expected CWT is 2.5 cm. From experimental observations (Sh76a), for a subject with CWT - 2.5 cm, one deduces a calibration factor 2.0×10^{-3} counts/photon for ^{103}Pd deposited in the lungs of the subject and a 20 cm dia phoswich placed centrally over the chest. The value of 1.4×10^{-3} counts/photon, obtained in the present work, for ^{103}Pd distributed uniformly in the lungs of the MIRD phantom and a 20 cm dia phoswich placed centrally over the chest, is indicative of CWT in excess of 2.5 cm. It is apparent that the MIRD phantom in its present form has rather excessive CWT, perhaps due to not fully appropriate representation of lungs inside the phantom thorax.

We may now proceed to characterise the MIRD phantom in terms of ESTT (Ru69) which is defined as the thickness of tissue-equivalent material which, when placed over a point source in a defined geometry, will cause equal attenuation of photons as occurs in the phantom. If a point ^{239}Pu source is placed on the detector (20 cm dia) axis and ordinary tissue is assumed to be present in the intervening space, then, making allowance for complete absorption of U_L x-rays (HVT in tissue = 0.6 cm) by rib bones covering 43 % of chest area, we readily note a counting efficiency of 23 cpm/uCi for a tissue thickness of 5.6 cm. A Monte Carlo calculation for these conditions gave 5.1 cm as thickness required to attain a similar counting efficiency. From these considerations and the calculated calibration factor for uniform ^{239}Pu source distribution (Table 5) for the MIRD phantom, one may conclude an ESTT between 5.1 and 5.6 cm. The calculated calibration factor for ^{103}Pd (Table 5) is 1.4×10^{-3} counts/photon which is similar to the experimentally observed value of 1.6×10^{-3} counts/photon for an ESTT of 5.6 cm (Sh76a). The ESTT of MIRD phantom may thus appear to be 5.6 cm. However, if one calculates the phantom ESTT from its body parameters, using the empirical relation suggested by Rundo et al (Ru69), (The relation was derived, fitting experi-

mental data from in-vivo calibration) a value (excluding rib thickness) of 4.5 cm is obtained. The value calculated from spectrum shape of 60 KeV photons (assuming saturated backscattering effect) works out to 4.5 cm.

Comparison with Other Models

Newton et al (Ne78b) have given a simple and perhaps anatomically more realistic semi-empirical model of human thorax to derive calibration factors for ^{239}Pu in lungs from studies with inhaled ^{103}Pd. They have calculated the value of R (= counts per Rh_{K_α} x-ray emitted from ^{103}Pd in lungs/Counts per U_L x-ray emitted from ^{239}Pu in lungs) as a function of chest wall thickness. The counting geometry considered is that of two phoswiches (12.7 cm dia each) placed centrally over each lobe of the lungs. Experimental observations made on subjects who had inhaled "mock-Pu" aerosol indicated that the counting efficiencies for ^{103}Pd in lungs of the subjects, for the twin detector geometry and the single detector geometry, described in this paper, were similar (within $\pm$ 20 %) (Ne78a). This suggests that insofar as the transmission of low-energy photons from human thorax is concerned, the same model results may be adopted for converting ^{103}Pd counting efficiency into that for ^{239}Pu. Since for the MIRD phantom the results presented here indicate a CWT of 3.2 cm, we find from Newton's model that the value of R corresponding to it is 5.14. Our results of Monte Carlo calculations for uniform source distribution in the lungs yield R = 6.3, suggesting phantom CWT 4 cm, assuming chest wall tissue to be water-equivalent in attenuation properties. A comparison of the results of our present work with Newton's model may be justified because of the similarities of cross-section data used at the desired photon energies and because a log u vs log E plot of data in Table 1 gives data almost similar to those used by Newton et al.

In addition, we calculated calibration factors for two 12.5 cm dia phoswiches - each located over one lobe of the lungs of the phantom with a uniform source distribution in the lungs. These were 34.4 cpm/uCi and 4550 cpm/uCi respectively for ^{239}Pu and ^{103}Pd. These data suggest a value of R = 7.58 which, according to Newton's model, would correspond to CWT very much in excess of 4 cm.

It is thus apparent that the MIRD phantom in its present form has rather excessive CWT and ESTT. As will be evident from the discussions earlier, there appear to be certain discrepancies regarding the estimates of these body build parameters for the MIRD phantom.

Comparison with Experimental Data

Apart from these discrepancies, there appear to be wide variations between experimental observations made on human volunteers who had inhaled mock-Pu aerosol on the one hand (Sh76a; Ne78a) and the results of Monte Carlo calculations for the MIRD phantom on the other. For the phantom calculations, identical responses are assumed for right and left lungs, whereas in measurements on human subjects carrying lung burdens of low-energy photon emitters such symmetric response is never observed (Sh76a; Ne78a; Ne78c). In addition, the general patterns of escape photons observed in human subjects are perhaps not reproducible in the MIRD phantom. For example, photon attenuation in the upper part of the phantom thorax is shown to be more than in the lower part. Furthermore, measurements on human subjects reveal that two 12.5 cm phoswiches, each located over one lobe of the lungs, yield a calibration factor for ^{103}Pd in lungs, which is similar (within ± 20%) to that of a single 20 cm dia phoswich located centrally over the chest, whereas the calculations for the MIRD phantom give for the two-detector system a response which is nearly twice of the latter system. In spite of these differences, we found that the calculations seem to support the experimental observations of Newton et al (Ne78a) in one respect, viz. no significant gain in figure of merit is achieved by increasing the diameter of the detector. These considerations prompt doubts as to the exactitude of the MIRD phantom for low-energy photon in-vivo spectrometry. Substantial improvisations may be needed in phantom representation. Perhaps, we may have to tread a path similar to that traversed by the experimentalists in the design of realistic phantoms for such calibration purposes.

CONCLUSION

The paper has described the details of a computer program designed to calculate the response of an external detector to a source of low-energy photons distributed in a selected manner in the lungs of a heterogeneous (MIRD) phantom. Predicted exit photon and the corresponding pulse-height spectra are presented for certain low-energy photon emitters. Comments are made on observed shifts in photopeakenergies. Calculated calibration factors are given for selected geometries together with photon escape efficiencies. An attempt has been made to characterise the MIRD phantom in its present form

for purposes of low-energy photon in vivo spectrometry. We do not consider the generalised predictions from the present work to be valid in actuality to human subjects. To enhance the suitability of the MIRD phantom for low-energy photon in vivo spectrometry, the need for modification of its present design is underscored and it is here that Dean's (De 76) work assumes considerable significance.

Acknowledgment

The authors wish to express their sincere thanks to D. Newton, AERE, Harwell and R.E. Goans, ORNL, Oak Ridge for their valuable suggestions.

REFERENCES

Ca59 Cashwell E.D. and Everett C.V., 1959. "A practical manual on Monte Carlo method for random walk problems", (Oxford: Pergamon Press)

Co68 Coleman W.A., 1968. "Mathematical verification of a certain Monte Carlo sampling technique and applications of the technique to a radiation transport problem", Nucl. Sci. & Engg. 32, 76

De76 Dean P.N., Griffith R.V. and Anderson, A.L., 1976. "Design criteria for phantoms for calibration of external detectors for the in vivo assay of plutonium", In: Diagnosis and Treatment of Incorporated Radionuclides, pp. 265-276 (Vienna: IAEA)

Fa74 Falk, R.B., 1974. "Calibration for inhaled radioactive material using a point source", Health Phys. 27, 557-563

Ga77 Garg S.P., 1977. "Ultrasonic measurements of chest wall thickness", Health Phys., 32, 34-39

Go76 Goans R.E. and Good W.M., 1976. "Calibration techniques and error analysis for phoswich counting of actinide nuclides at Oak Ridge National Laboratory", Battelle Northwest Laboratory report BNWL-2089, p. 19

Ha77 Haridasan T.K., Sharma R.C. and Somasundaram, S., 1977. "Ultrasonic measurements of chest wall thickness in Indian subjects", Paper presented at Fourth Annual Conference on Radiation Protection, Madras, March 12-14

Hu69 Hubbell J.H., 1969. "Photon cross-sections, attenuation coefficients and energy absorption coefficients from 10 KeV to 100 GeV", National Bureau of Standards Reference Data Series 29

Ju72 Julius H.W. and Verhoef C.W., 1972. "Calibration of whole-body counting equipment by using computers instead of phantoms", In: Assessment of Radioactive Contamination in Man, pp. 201-213 (Vienna: IAEA)

Ne78a Newton D., Fry F.A., Taylor B.T., Eagle M.C. and Sharma R.C., 1978. "Interlaboratory comparison of techniques for measuring lung burdens of low energy x-ray emitters", Health Phys. 35, 751-771

Ne78b Newton D., Taylor B.T. and Anderson A.L., 1978. "X-ray counting efficiencies for plutonium in lungs derived from studies with inhaled Pd-103", Health Phys., 34, 573-585

Ne78c Newton D., 1978. AERE Harwell (Personal Communication)

Ru69 Rundo J., Rudran K. and Taylor B.T., 1969. "Effective tissue thicknesses for external counting of low-energy emitters in lung", Health Phys. 17, 155-157

Sc77 Scott L.M., Warner G.G. and Poston J.W., 1977. "Theoretical evaluation of optimum detector size and positioning for low energy in vivo gamma spectrometry", Health Phys. 33, 583-593

Sh72a Sharma R.C., Garg S.P. and Somasundaram S., 1972."Monte Carlo calculations for thin NaI(Tl) crystal at energies below 100 eV", Nucl. Instru. & Meth. 101, 413

Sh72b Sharma R.C., Nilsson I and Lindgren L., 1972. "A twin large area proportional flow counter for the assay of plutonium in human lungs", Aktibolaget Atomenergie report AE-463

Sh74 Sharma R.C., Somasundaram S., Surendran T., Kapur D.K. and Garg S.P., 1974 "Plutonium in human lungs: Assessment with thin NaI(Tl) detector systems", Bhabha Atomic Research Centre report BARC-748

Sh76a Sharma R.C., Somasundaram S., Kotrappa P., Haridasan T.K., Surendran T., Krishnamachari G., Bhanti D.P. and Pimpale N.S., 1976. "Assessment of chest burdens of plutonium", In: "Diagnosis & Treatment of Incorporated Radionuclides", pp. 177-201 (Vienna: IAEA)

Sh76b Sharma R.C., 1976. In: "Diagnosis & Treatment of Incorporated Radionuclides", Discussion pp. 281-284 (Vienna: IAEA)

Sh77 Sharma R.C., Somasundaram S., Unnikrishnan K. and Datta S., 1977. "Spectrum shapes of low energy photon sources", National Bureau of Standards Special Publication 461, pp. 188-192

To76 Tomlinson F.K., 1976. "Plutonium - 239 lung counting with phoswich detectors", In: Diagnosis & Treatment of Incorporated Radionuclides", pp. 237-247 (Vienna: IAEA)

Zi61 Zimmermann W., 1961. "Evaluation of photopeaks in scintillation gamma-ray spectrometry", Rev. Sci. Instr. 32, 1063

Table 1, Mass attenuation coefficients for tissue and bone used in the calculations

Photon Energy (KeV)	Photoelectric (μ_p)		Total (μ_t)	
	Tissue+ ($cm^2.g^{-1}$)	Bone ($cm^2.g^{-1}$)	Tissue+ ($cm^2.g^{-1}$)	Bone ($cm^2.g^{-1}$)
10	4.78	19.78	4.99	20.00
15	1.27	5.95	1.48	6.15
20	0.505	2.49	0.711	2.68
30	0.138	0.716	0.338	0.907
40	0.055	0.293	0.248	0.478
50	0.027	0.147	0.214	0.327
60	0.015	0.084	0.197	0.258
80	0.006	0.035	0.179	0.200
100	0.003	0.017	0.168	0.174
150	0.000	0.005	0.149	0.147
200	0.000	0.002	0.136	0.132

The corresponding linear attenuation coefficients are obtained by multiplying these values with densities ($g.cm^{-3}$) which for ordinary tissue and bone are 1.0 and 1.8 respectively.

+) Linear attenuation coefficients for lung tissue are obtained by multiplying these values with lung density (0.3 $g.cm^{-3}$)

Table 2, Mass attenuation coefficients of tissue calculated at intermediate photon energies from linear interpolation and log-log plots

Photon Energy (KeV)	Photoelectric (μ_p)		Total (μ_t)	
	Linear	Log-Log	Linear	Log-Log
13.6	2.25	1.81	2.46	2.00
17.2	0.93	0.82	1.14	1.04
20.2	0.497	0.489	0.701	0.697
22.8	0.402	0.334	0.571	0.551
26.4	0.272	0.210	0.474	0.421

Table 3, Calculated iodine escape peak to photopeak ratios for a 3 mm thick NaI(Tl) crystal at different energies for the case of good geometry

Photon Energy (KeV)	Escape/photopeak ratio x 10^{-1}
35	3.07
40	2.30
45	1.85
50	1.51
55	1.20
60	1.00
65	0.84
70	0.71
75	0.61
80	0.52
90	0.43
100	0.40
>100	0.40

Table 4, L x-ray energies and their intensities in percentage of disintegrations from parent actinide nuclide

Parent nuclide	L_α		L_β		L_γ	
	Energy (KeV)	Intensity (%)	Energy (KeV)	Intensity (%)	Energy (KeV)	Intensity (%)
^{239}Pu (U_L x-ray)	13.6	1.82	17.2	2.16	20.2	0.53
^{238}Pu (U_L x-ray)	13.6	4.15	17.2	5.61	20.2	1.36
^{241}Am* (Np_L x-ray)	13.94	13.2	17.75	19.25	20.8	4.85
^{244}Cm (Am_L x-ray)	14.28	3.86	18.3	4.3	21.4	1.03
^{246}Cm (Am_L x-ray)	14.28	3.33	18.3	3.71	21.4	0.86
^{250}Cf (Cm_L x-ray)	14.96	3.27	19.43	3.85	22.73	0.85

* In addition 26 KeV gamma has 2.5 % and 59.6 KeV has 35.9 % abundance. Electron capture radionuclide ^{103}Pd emits Rh K_α and Rh K_β x-rays of energies 20.2 and 22.8 KeV with intensities of 65 % and 15 % respectively.

Table 5, Calculated calibration factors (cps/uCi) for a single 20 cm dia phoswich detector placed centrally over the chest of MIRD phantom for two kinds of source distribution in the lungs

Radionuclide	Calibration factor (cps/uCi) for full x or gamma spectra	
	Uniform distribution in lung	Point source at the centre of each lung*
^{239}Pu	22.3	18.3
^{238}Pu	57.7	49.3
^{241}Am	48837+	58985+
^{244}Cm	606.4++	686.0++
^{246}Cm	79.6	66.8
^{250}Cf	105.3	97.7
^{103}Pd	2433	2723

* Coordinates: ± 8.5, 0, 55.5

+ For 59.5 KeV gamma-rays only

++ For (X + 26 KeV) gamma-ray regions only.

Table 6

Calibration factors for ^{239}Pu and ^{103}Pd point sources at three defined locations (S1, S2 and S3) inside the lung

(Detector geometries are indicated by the coordinates of detector centres)

Detector location & diameter	Calibration factor (cpm/μCi) for ^{239}Pu point source at			Calibration factor (cpm/μCi) for ^{103}Pd point source at		
	S1	S2	S3	S1	S2	S3
D1 (12.5 cm)	17.93	21.70	3.56	2403	2161	725
D2 (12.5 cm)	16.36	41.45	31.80	1835	4745	3831
D3 (12.5 cm)	2.54	21.10	60.30	562	1317	6658
D2' (20 cm)	22.44	54.20	65.86	3345	6886	7581

Coordinates:

Detector centre D1 (8.5, -10, 61.5) D2 & D2' (8.5, -10, 55.5) D3 (8.5, -10, 49.5)
Source S1 (8.5, 0, 61.5) S2 (8.5 0, 55.5) S3 (8.5, 0, 49.5)

Table 7, Calibration factors for ^{239}Pu and ^{103}Pd point sources at five locations inside lung (The detector is a 20 cm dia phoswich placed centrally over the chest as shown in Fig. 1)

Source location	Calculated calibration factor (cpm/uCi	
	^{239}Pu	^{103}Pd
ST	0.045	137
S1	9.83	1071
S2	18.34	2723
S3	16.6	2070
SB	2.62	611

Coordinates: Source ST (8.5, 0, 67.5)
SB (8.5, 0, 43.5)
Detector Centre DO (0, -10, 55.5)

Table 8

Escape efficiencies, expressed in percentage, of source photons, escaping from different parts of MIRD phantom (Uniform distribution of source photons in lungs is assumed. The results from Scott et al (Sc 77) are given in parentheses).

Photon Energy (KeV)	Front*		Back*		Sides**		Total Phantom		
	Uncollided	Total	Uncollided	Total	Uncollided	Total	Uncollided	Total	Ratio $\frac{\text{Total}}{\text{Uncollided}}$
185	8.36 (9.30)	27.69	9.40 (10.195)	29.39	8.62 (9.353)	27.16	26.38 (28.848)	84.24	3.19
90	6.70 (7.586)	23.65	7.32 (8.007)	25.29	6.95 (7.26)	22.39	20.97 (22.85)	71.33	3.40
53	5.19 (5.93)	14.97	5.83 (6.133)	16.29	5.03 (5.448)	14.51	16.05 (17.51)	45.77	2.85
16	0.045 (0.051)	0.06	0.056 (0.056)	0.065	0.009 (0.012)	0.011	0.11 (0.119)	0.137	1.27

* Right arm removed ** Both arms of phantom removed

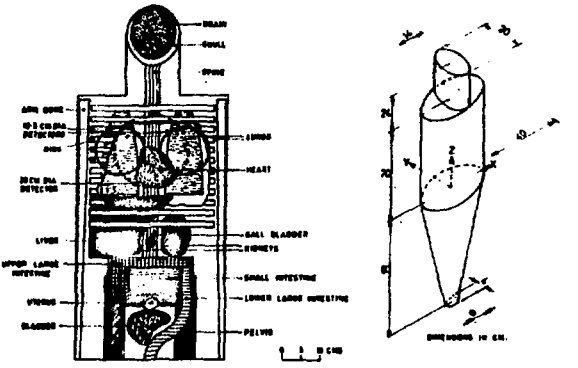

FIG. 1:- ANTERIOR VIEW OF THE PRINCIPAL ORGANS IN TRUNK OF THE MIRD PHANTOM AND ITS OUTLINE. ALSO INDICATED ARE THE POSITIONS OF PHOSWICH DETECTORS AND CO-ORDINATE AXES.

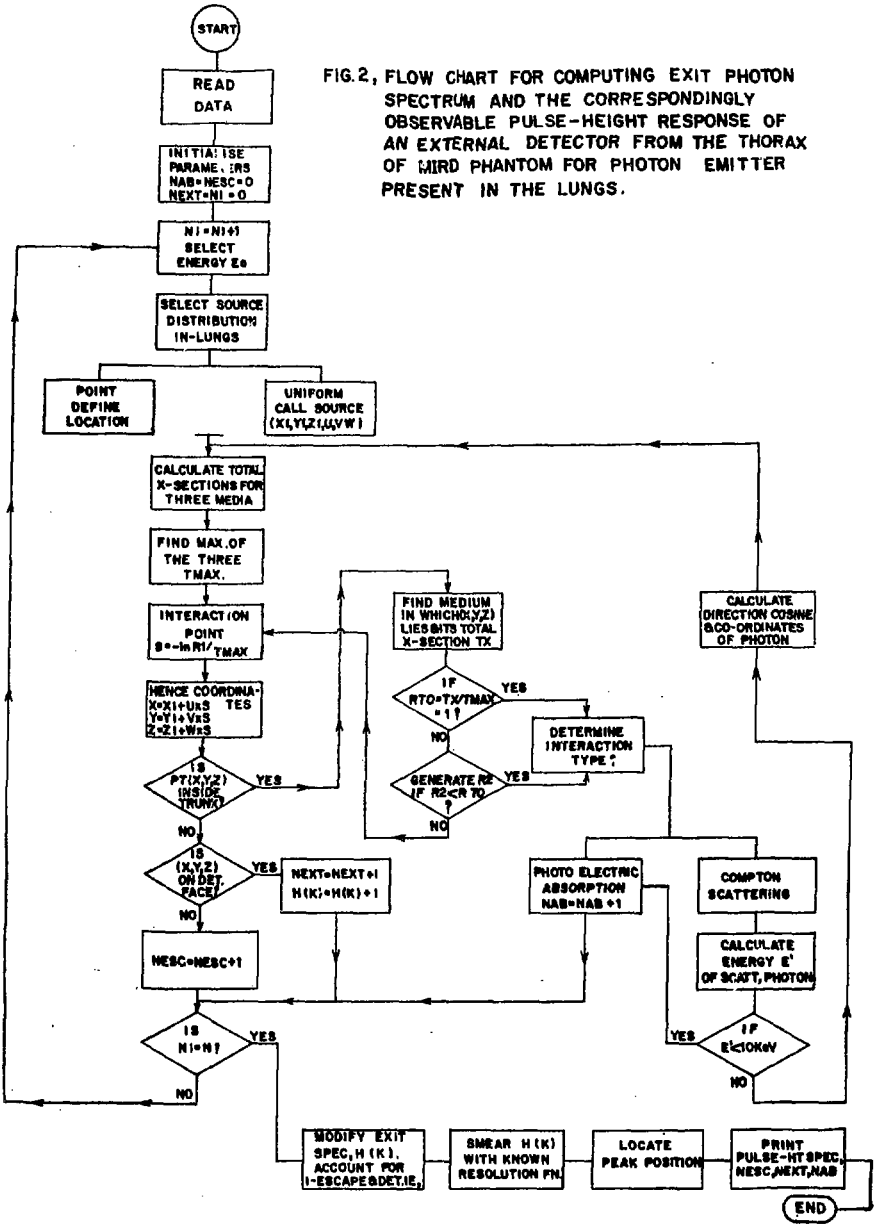

FIG. 2, FLOW CHART FOR COMPUTING EXIT PHOTON SPECTRUM AND THE CORRESPONDINGLY OBSERVABLE PULSE-HEIGHT RESPONSE OF AN EXTERNAL DETECTOR FROM THE THORAX OF MIRD PHANTOM FOR PHOTON EMITTER PRESENT IN THE LUNGS.

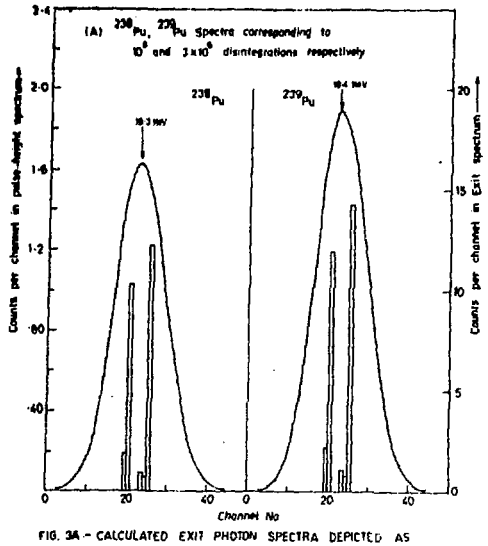

FIG. 3A – CALCULATED EXIT PHOTON SPECTRA DEPICTED AS HISTOGRAMS AND THE RESULTANT PULSE-HEIGHT SPECTRA FROM A 20cm DIA PHOSWICH SHOWN AS SMOOTH CURVES FOR ^{238}Pu AND ^{239}Pu UNIFORMLY DISTRIBUTED IN THE LUNGS OF MIRD PHANTOM. THE CHANNEL WIDTH IS 0·6KeV/CHANNEL.

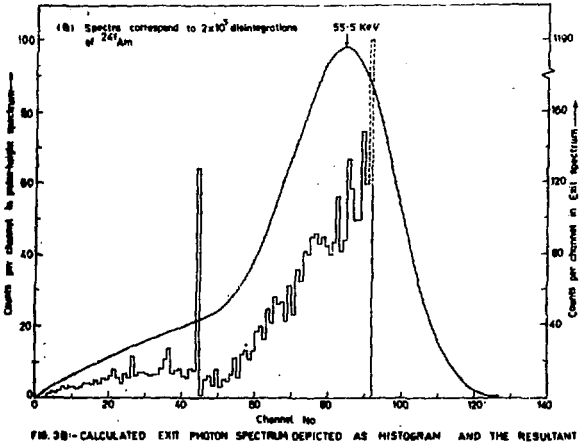

FIG. 3B – CALCULATED EXIT PHOTON SPECTRUM DEPICTED AS HISTOGRAM AND THE RESULTANT PULSE-HEIGHT SPECTRUM FROM A 20cm. DIA. PHOSWICH SHOWN AS SMOOTH CURVE FOR ^{241}Am UNIFORMLY DISTRIBUTED IN THE LUNGS OF MIRD PHANTOM THE CHANNEL WIDTH IS 0·8KeV/CHANNEL.

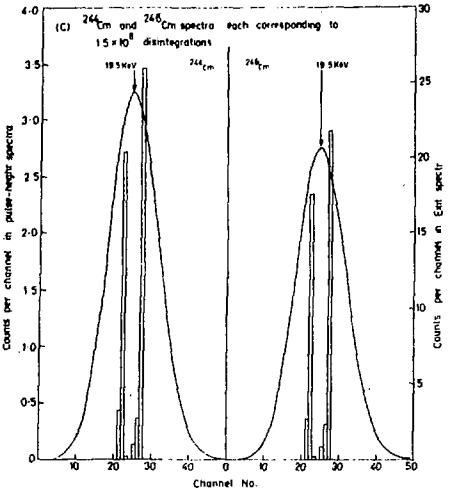

FIG. 3C – CALCULATED EXIT PHOTON SPECTRA DEPICTED AS HISTOGRAMS AND THE RESULTANT PULSE-HEIGHT SPECTRA FROM A 20cm DIA PHOSWICH SHOWN AS SMOOTH CURVES FOR ^{244}Cm AND ^{246}Cm UNIFORMLY DISTRIBUTED IN LUNGS OF MIRD PHANTOM CHANNEL WIDTH IS 0·6 KeV / CHANNEL

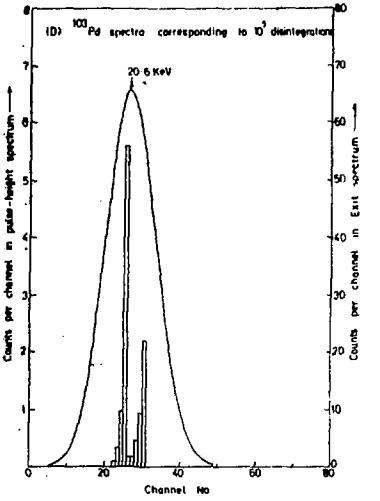

FIG 3D - CALCULATED EXIT PHOTON SPECTRUM DEPICTED AS HISTOGRAM AND THE RESULTANT PULSE-HEIGHT SPECTRUM FROM A 20cm DIA PHOSWICH SHOWN AS SMOOTH CURVE FOR ^{103}Pd UNIFORMLY DISTRIBUTED IN THE LUNGS OF MIRD PHANTOM THE CHANNEL WIDTH IS 0·6 KeV/ CHANNEL

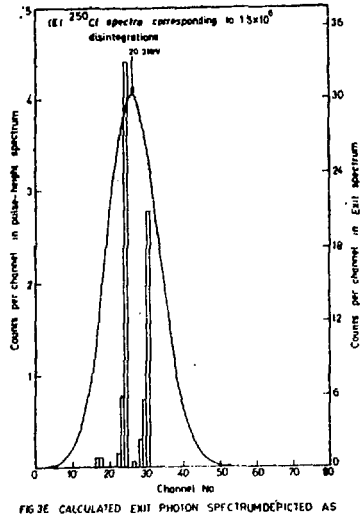

FIG 3E CALCULATED EXIT PHOTON SPECTRUM DEPICTED AS HISTOGRAM AND THE RESULTANT PULSE-HEIGHT SPECTRUM FROM A 20 cm DIA. PHOSWICH SHOWN AS SMOOTH CURVE FOR ^{250}Cf UNIFORMLY DISTRIBUTED IN LUNGS OF MIRD PHANTOM. CHANNEL WIDTH IS 0.6 KeV/CHANNEL

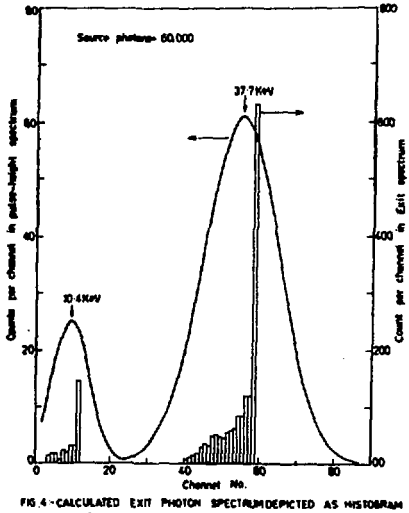

FIG 4 - CALCULATED EXIT PHOTON SPECTRUM DEPICTED AS HISTOGRAM AND THE RESULTANT PULSE-HEIGHT SPECTRUM FROM A 20cm DIA. PHOSWICH SHOWN AS SMOOTH CURVE FOR A 40 KeV MONOENERGETIC PHOTON SOURCE UNIFORMLY DISTRIBUTED IN LUNGS OF MIRD PHANTOM

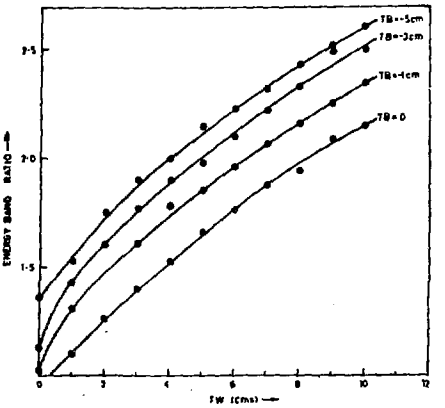

Fig.5A-Monte Carlo predictions of ratio of counts in two energy bands of pulse-height spectrum of 60 KeV photons for phoswich detector, the absorber-scatterer being Water. A point source is assumed to be located on detector axis. TW and TB indicate thicknesses of water on top and behind the point source respectively.

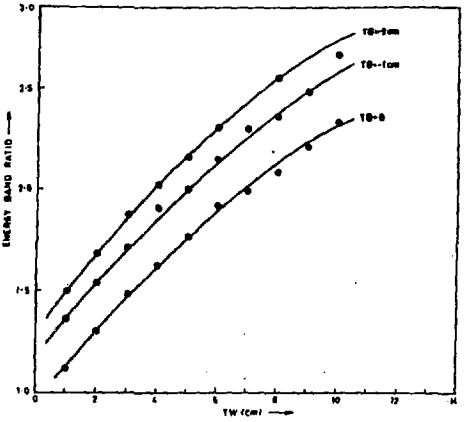

Fig.5B-Monte Carlo predictions of ratio of counts in two energy bands of pulse-height spectrum of 60KeV photons for phoswich detector, the absorber-scatterer being lucite (perspex). A point source is assumed to be located on detector axis. TW and TB indicate thicknesses of lucite on top and behind the point source respectively.

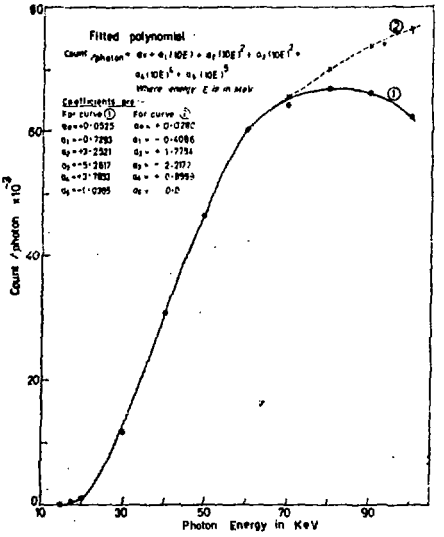

FIG. 6 - VARIATION OF CALIBRATION FACTOR (count/photon) FOR THE MIRD PHANTOM AS A FUNCTION OF INITIAL PHOTON ENERGY UNIFORM DISTRIBUTION OF PHOTON SOURCE IN THE LUNGS AND A 20cm. DIA. PHOSWICH CENTRALLY OVER CHEST ARE ASSUMED. RESULTS ARE WITH (—) AND WITHOUT (----) CORRECTION FOR THE VARIATION IN INTRINSIC EFFICIENCY OF THE DETECTOR.